Available online at www.sciencedirect.com
ScienceDirect
Journal of Photochemistry and Photobiology A: Chemistry 196 (2008) 127–137
Journal of Photochemistry and Photobiology A:Chemistry
www.elsevier.com/locate/jphotochem

Photon-driven electron and atomic processes on solid-state surface in photoactivated spectroscopy and photocatalysis

Andrei A. Lisachenko *

V.A. Fock Institute of Physics, St. Petersburg State University, Oulianovskaja 1, St. Petersburg, Peterhof 198504, Russia

Available online 9 February 2008

Abstract

Several results of "spectro-manometric" investigations of photoinduced processes in gas–solid systems pioneered by A.N. Terenin in the Leningrad State University which gave rise to the "photonics of heterogeneous systems" continued by his disciples are discussed. The step-by-step experimental investigations of mechanisms of interrelated processes in electronic and atomic subsystems on UV–vis illuminated surface of wide-bandgap oxides are presented. A variety of complementary experimental methods such as the mass-spectrometry, the optical, luminescence and ESR spectroscopies, and the UV-photoelectron spectroscopy have been adapted to carry out in situ investigations in three phases: gas–adsorbate–surface.

The primary acts of electron subsystem excitation in the sub-bandgap range are the spectral-selective and site-sensitive excitations of F- and V-type centers. The role of photoadsorption and photodesorption of oxygen as relaxation channels competing with radiative and non-radiative decay is treated. Spectral and kinetic parameters of photoexcited centers and structures of adsorbate complexes are determined. Highly active oxygen species arise at photoactivated surface, allowing oxygen vacancies to form or to heal and also to oxidize a number of adsorbed molecules.

Using the time-of-flight (TOF) spectroscopy, the composition and the kinetic energy distributions of photodesorbed particles are analyzed for to obtain the dynamics of bond rearrangements and bond breaking. The results are discussed in the framework of a charge transfer approach in excited clusters. The potentialities of the presented results for probing and characterization of the electronic and atomic structure of active sites on the surface, as well as for a regulation of a number and a composition of surface defects are discussed.

We have demonstrated on an example of NO_x/Al_2O_3 and $(NO + CO)/TiO_2$ systems that proper defects of F, F^+ and V-type can be used for sensitization of photocatalysts to a long-wave spectral range.

Keywords: Surface photochemistry; Simple molecules; Wide-bandgap oxides; Point defects; Spectral sensitization

1. Introduction

In 1930s professor A.N. Terenin started a pioneering research of adsorbed molecules using various optical methods [1]. Further development of these works was characterized by a shift from optics to photochemistry of the adsorbed phase. The use of UV-irradiation for the electronic excitation enables one not only to deduce from the spectral changes the perturbations, experienced by an adsorbed molecule in the surface field, but also to obtain an information about the nature and chemical activity of excited state, which is attained by the vertical Franck-Condon optical transition. The effects in which an UV-irradiation of the gas–solid interface entails an excitation of the electronic subsystem and leads to a breaking of already existing interatomic bonds or to a formation of new bonds in adsorbed phase were investigated [2].

Professor Terenin had discovered the photoactivated desorption and the dissociation of adsorbed molecules by the gas pressure monitoring over the illuminated surface. Terenin had emphasized the advantages of this "spectro-manometric" method [3]: "In comparison with the determination of absorption IR or UV or UV–vis spectra of adsorbed molecules this method has the following advantages: (1) only photochemically active regions are thus isolated from the broad, mostly unspecific continuous absorption spectrum; (2) the method is by far more sensitive, reaching a sensitivity of 10^{-5} monolayer since it is registering a positive effect, instead of a relative change of the light intensity which is exceedingly small for

* Tel.: +7 812 428 43 08; fax: +7 812 428 72 00.
E-mail address: lisachen@photonics.phys.spbu.ru.

1010-6030/$ – see front matter © 2008 Elsevier B.V. All rights reserved.
doi:10.1016/j.jphotochem.2008.01.017

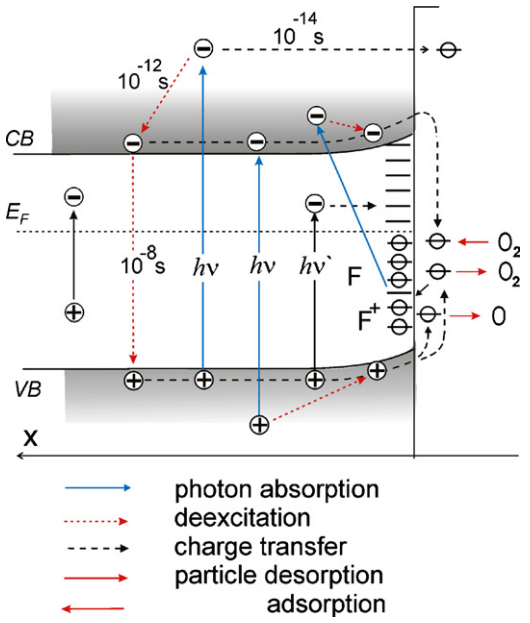

Fig. 1. Time scales of the modes of electronic excitations and relaxation.

adsorbed molecules; (3) the method can be used with opaque objects."

Towards sixties such spectro-manometric researches were widely performed in many countries [4]. The works of Terenin are discussed in the overview [5]. Since the information about *what happens* leads to a lot of questions about *how* and *why it happens*, Terenin elaborated a program of a complex experimental step-by-step investigation of photophysical and photochemical processes from the first stage – the absorption of a light quanta – to the final stage – the breaking or formation of new bonds. This line of investigations he called "Photonics" [6].

Photonics has occupied an important place among other directions developed by Terenin, i.e. optical spectroscopy of adsorbed molecules, UV photoelectron spectroscopy, photoionisation mass-spectrometry, all of them being widely used today.

The "Photonics of heterogeneous systems" designates a thorough study of electronic and atomic processes in three phases: solid, adsorbed and gas. This study gave rise to a novel original approach to a fundamental investigation and characterization of the gas–solid interface called the "photoactivation spectroscopy of adsorbed molecules", and included works on photocatalysis.

The results are also of great importance for applied problems. We can note among them the development of advanced technologies of preparation and characterization of surfaces with prescribed physical and chemical properties: the photon-driven annealing, etching, epitaxy, lithography, etc.; the solar to chemical energy conversion by means of photocatalytical reactions.

A further investigation of the phenomena discovered by Terenin was started under his supervision and is continued up to now by his disciples on the basis of the latest advances in the surface science. Some results concerning gas–solid systems, obtained in the laboratory of Photonics founded by Terenin in the Institute of Physics of the St. Petersburg State University are discussed in the present paper.

2. Photoactivation spectroscopy in the gas–solid system

The major part of interplayed photon-driven physical and chemical processes on the surface (photodesorption, photoadsorption, photochemical reactions) are not elementary processes

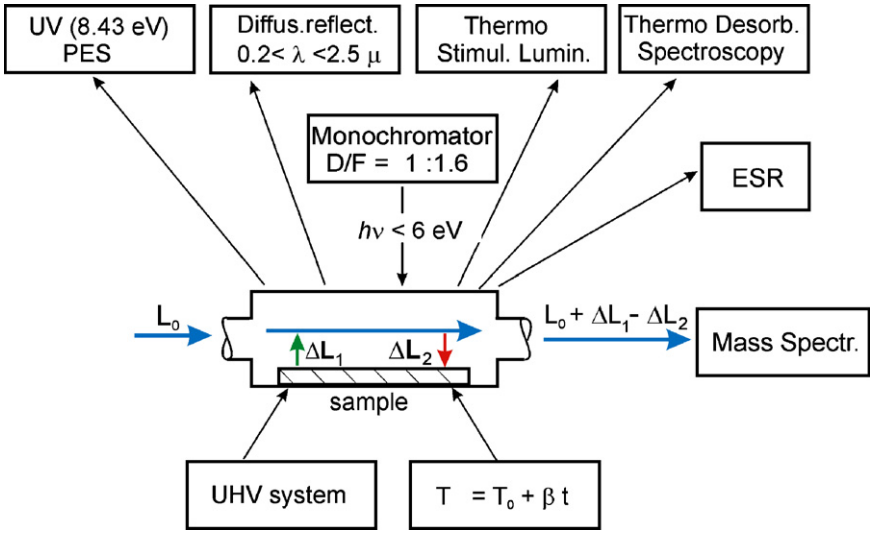

Fig. 2. Experimental setup for in situ diagnostics and photocatalytic experiments. L_0 is the initial gas flow, ΔL_1 is the gas flow from the sample due to photodesorption, ΔL_2 is the gas flow onto the sample due to photoadsorption. UV (8.43 eV) PES is the photoelectron spectrometer with Xe resonance source, Diff. reflect. $200 < \lambda < 2500$ nm is the spectrophotometer for optical absorption measurements in the UV–vis–NIR range of $200 < \lambda < 2500$ nm, Thermo Stimul. Lumin. is the spectrometer for analysis of spectra of excitation and emission of thermoactivated luminescence. Thermo Desorb. Spectroscopy is realized in "flow-through" regime. Monochromator is of original construction with aperture 1:1.6 for spectral range of $200 < \lambda < 800$ nm, ESR is the electron spin resonance spectrometer; Mass Spectr. is the mass-spectrometer; UHV system is Ultra High Vacuum system. $T = T_0 + \beta t$ is the system for variation of the sample temperature with constant rate $0.1 < \beta < 0.5$ K/s in the range of $300 < T < 1000$ K, for TDS and TSL measurements.

and should be described within a three-step model: (1) fast initial electronic excitation → (2) energy or charge transfer → (3) chemical bonds breaking and/or forming at the surface.

As soon as the existence of the quantum photo-driven effect in a system being studied is proved, three key questions arise.

What is the nature of the photon absorption in the UV–vis range ($1 < h\nu < 6$ eV)? How the excitation energy is transferred to an active site and what are the bonds broken (or formed) in the adsorbate–surface system, entailing the photon-driven adsorption, desorption or chemical reactions? What is the molecular dynamics of bond breaking and formation?

The main part of investigations over the world deals with metals or semiconductors excited in the fundamental absorption region [7], while a photoexcitation of semiconductors and insulators in the sub-bandgap absorption region is poorly studied.

In the present paper the key features of photonics of the gas–solid interface are revealed and exemplified by a number of heterogeneous systems: simple molecules (H_2, O_2, CO, CO_2, NO, N_2O) adsorbed on wide-bandgap metal oxides (BeO, Al_2O_3, MgO, ZnO and TiO_2). The emphasis is focused on the sub-bandgap excitations. In such systems the gas molecules are transparent, and the photon absorption in the $1 < h\nu < 6$ eV region is defined by the metal oxides (semiconductors or insulators). The following excitations of the electron subsystem of a solid are possible: (a) the interband excitation resulting in the electron–hole generation, (b) the excitations of local states (surface or bulk point defects), and (c) the photoinduced charge transfer between local states and the valence band or the conduction band.

The interband absorption is not possible in BeO, Al_2O_3, MgO in $1 < h\nu < 6$ eV region, because the bandgaps in these oxides are equal to 10.5, 9.3 and 7.8 eV, respectively. So only mechanisms (b) and (c) are feasible. The absorption of these nominally pure oxides in the $1 < h\nu < 6$ eV region is due to local centers of F-type (oxygen vacancies, empty or filled by one or two localized electrons), V-type centers (a metal vacancy having localized one or two holes) and numerous low-coordinated ions on the surface. In ZnO and TiO_2 all the three absorption modes (a, b, and c) are possible.

In Fig. 1 the modes of electronic excitations together with typical time scales are indicated: 10^{-14} s for the electron transport to the surface, 10^{-12} s for the intraband relaxation, and 10^{-8} s for the interband relaxation. The relaxation times for local long-living states on the surface can attain up to 10^3 s. The chemical channels of electron energy relaxation, such as the adsorption and desorption of molecular and atomic oxygen, are also shown. The latter time interval can vary in an extremely wide range, i.e. from 10^{-13} to 10^5 s. These are the time scales that are key parameters of the excited system determining the power of different channels of energy evolution.

2.1. Experimental methods and results

Various complementary experimental methods such as: mass-spectrometry, thermodesorption (TDS) spectroscopy, optical (diffusion reflectance) and electron spin resonance (ESR) spectroscopies, thermostimulated photoluminescence (Thermo Stimul. Lumin), as well as UV (8.43 eV) photoelectron spectroscopy (UPS) have been adapted to carry out *in situ* investigations in three phases: gas, adsorbate and solid state [8] (Fig. 2).

Single crystals and dispersed powders of nominally pure oxides were irradiated by monochromatic light with the power density of $\sim 1 \times 10^{-3}$ to 1×10^{-1} W/cm^2 in UHV $\sim 10^{-9}$ Torr or in a flow of pure gases under a controllable pressure of 10^{-8} to 10^{-2} Torr. For TOF measurements a Nd laser ($P/S = 10^4$ to 10^7 W/cm^2, $\tau = 10$ ns) was used. The experimental devices and procedures are described elsewhere [8].

The main feature of the setup, depicted in Fig. 2, is the use of the "flow-through" silica reactor connected with a mass-spectrometer. Replacing of an integral manometer by a mass-spectrometer allowed to measure the molecular composition, the pressure and the value of the gas flow over a sample. It enables one to analyze the photodesorption under UHV, as well as the photoadsorption and the photochemical reactions in a flow-through regime. The use of the isotope enriched molecules reveals the dynamics of photodesorption/photoadsorption processes [9].

2.2. Spectro-kinetic investigation in the gas phase

As it was shown by Terenin [1], bond rearrangements in the adsorbate–surface system result in a violation of a gas–surface equilibrium and are manifested in the change of the pressure and/or the composition of the gas phase. In our experiments a pure (99.99%) oxygen flow was admitted over the carefully cleaned sample under the controllable dynamical pressure of 10^{-8} to 10^{-3} Torr. The sample was irradiated with a monochromatic light tuned in the spectral range of $200 < \lambda < 600$ nm ($6 > h\nu > 2$ eV) with a power density of the order of 1 mW/cm^2. For the "flow-through" regime the rate dn/dt of photoadsorption (photodesorption) per unit area can be found from the expression $-\frac{dn}{dt} = \frac{1}{A}\left(\frac{d\Delta N}{dt} + \frac{\Delta N}{t_p}\right)$ where t_p being the characteristic pump-off time, $N_0 = L_0 t_p$ is the initial number of molecules above the sample.

The quantum yield Φ for photoadsorption or photodesorption is $\Phi = (dn/dt)\,(1/k_\lambda I_{h\nu})$ molecule/quantum, where k_λ is the absorption coefficient of the sample and $I_{h\nu}$ is the light intensity. The experimental results for [O_2–Al_2O_3] system are given in Fig. 3.

The illumination abruptly shifts the initial dynamical gas–surface equilibrium, and the sign of ΔL depends on the light spectral region. So, for oxygen–Al_2O_3 system in the spectral region $h\nu > 4$ eV an irreversible photoadsorption is observed, while the opposite effect – a reversible photodesorption – takes place at $h\nu < 3$ eV. At middle energies both effects coexist. Three features of the kinetic curve are of special interest:

- the part of stationary rate of photoadsorption (a);
- the region of the kinetic curve after cutting off the illumination (a–b) which characterizes the "memory effect" [10], describing the interaction of oxygen molecules with long-lived excitations;

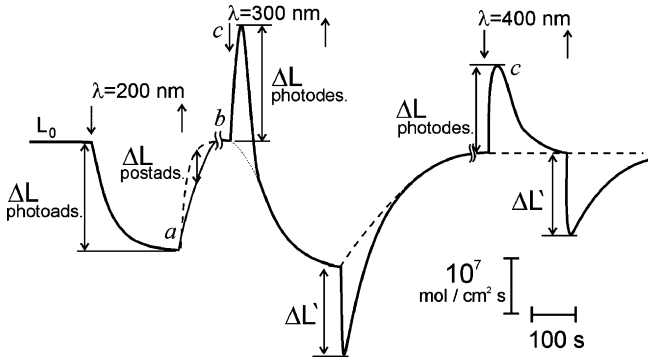

Fig. 3. Effect of illumination on the change of O_2 flow over Al_2O_3.

Table 1
Relaxation channels of photogenerated centres z*

$z+h\nu \rightarrow z^*(k_g)$	$z^* \rightarrow z+h\nu'$	Radiative decay	τ_1
	$z^* \rightarrow z+h\omega$	Non-radiative thermo-activated decay	
	$z^*+M \rightarrow zM$	Photoadsorption	τ_2

- the maximum (c) at the initial moment of illumination in the long-wave region, giving the maximal rate of photodesorption.

It is reasonable to describe the kinetics under the assumption that the effects are caused by an interaction of gas (photoadsorption) or adsorbed (photodesorption) molecules with photogenerated local centers. Three channels of excitation decay are presented in Table 1. They are the recombination of photogenerated centres z^* via radiative and non-radiative decay, as well as the adsorption/desorption of molecules on/from these centers.

If r_g is the rate of photogeneration of the active centers z^*, then $r_g = dz/dt = k_g z_i I_{h\nu}$, z_i being the concentration of eventual centers of photoadsorption. Their typical concentration does not exceed 10^{11} cm^{-2}. The portion "a" of the curve in Fig. 3 represents the rate of the stationary photoadsorption when r_g is equal to the sum of the decay rate of active centers $k_1 z^*$ and the rate of reaction of gas molecules with active centers $k_2 p z^*$. The rate of photoadsorption dn/dt in this case is proportional to $r_g kp/(kp+1)$, where $k = k_2/k_1$ or $dn/dt = \alpha r_g \tau_1/(\tau_1+\tau_2)$, where $\tau_1 = 1/k_1$ is the lifetime of an active center relative to the decay, and $\tau_2 = 1/k_2 p$ is the lifetime relative to photoadsorption. If $\tau_2 \ll \tau_1$ ($k_2 p \gg k_1$), then $dn/dt \approx \alpha r_g$, i.e. the rate of photoadsorption is independent of p value and is equal approximately to the rate of centers 'photogeneration. This is the case of "high" pressure. At "low" pressure $\tau_2 \gg \tau_1$ ($k_2 p \ll k_1$) and $dn/dt = \alpha r_g p k_2/k_1$, i.e. the rate of photoadsorption is proportional to p. The value of τ_1 attains 10^4 s in UHV while in oxygen it drops to 1–10 s depending on the oxygen pressure.

The photoadsorption is practically irreversible, i.e. photoadsorbed molecules do not desorb when illumination is cut off (Fig. 3, curve a). On the contrary, photodesorption is reversible: the illumination being cut off, desorbed molecules readsorb onto the surface (Fig. 3, curve d), i.e. the adsorption centers are delivered but are not destructed during the photodesorption. Indeed, photoadsorption is the most efficient relaxation channel of all

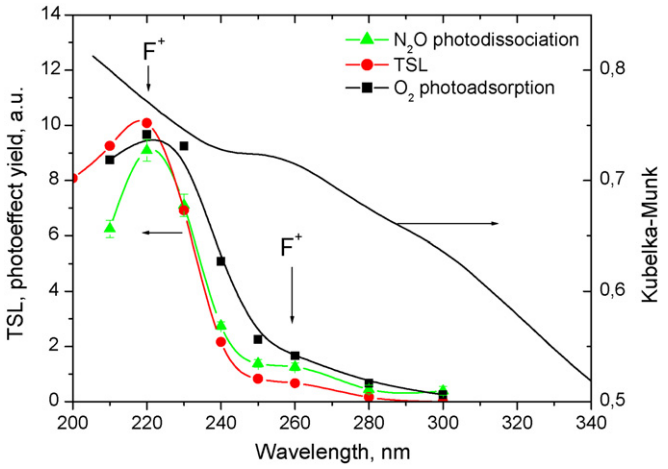

Fig. 4. Spectral efficiencies of O_2 photoadsorption (squares), N_2O photodissociation (triangles) and TSL photoexcitation (circles). Spectral absorbance is represented by Kubelka-Munk function.

the three listed in Table 1, nevertheless the photodesorption is a channel of energy relaxation of the excited surface as well.

The existence of long-lived excitations proves that the excited state of the surface is metastable due to the deviation of the charge equilibrium, and the photoadsorption/desorption of oxygen is one of competing channels of the energy relaxation. Hence, the analysis of the dependence $dn/dt \propto p$ in combination with the luminescence kinetics allows one to calculate k_g, k_1 and k_2, as well as τ_1, τ_2 and σ (σ is the cross-section for the capture of an oxygen molecule by an active center) [7].

For Al_2O_3 samples the values of σ of the order of 4×10^{-18} cm^{-2} have been obtained, the values of τ_1 were of the order of 10^{-5} s for the main part of the centers, attaining 10^2 to 10^3 s for 5% of them. For a number of studied oxides the kinetic parameters of active centers varied in a vide range: $10^{-5} < \tau_1$, $\tau_2 < 10^3$ s, $10^{-18} < \sigma < 10^{-16}$ cm^2, $10^{-6} < \Phi_{pd} < 10^{-4}$ molecule/quantum, $10^{-5} < \Phi_{pa} < 10^{-4}$.

The photoadsorption is a spectrally selective process. The spectral maximum of photoadsorption efficiency on Al_2O_3 is centered at ~230 nm, and has a shoulder at ~260 nm (Fig. 4) that coincides with the optical absorption of F^+-centers [11]. It should be noted that as early as in the thirties Kassparov and Terenin had for the first time discovered the NH_3 photodecomposition over Al_2O_3 illuminated by 230 nm photons, beyond the fundamental absorption region [2].

The spectral efficiency of oxygen photodesorption and CO photoadsorption is shifted to a long-wavelength region in the absorption band of V-centers [11]. So photodesorption is activated by a photoexcitation of the hole V-type centers (not of the electron F-type centers).

The spectral efficiency of a preliminary irradiation in UHV (the "memory effect") coincides with the spectral band of photoadsorption efficiency suggesting that the nature of short-lived and long-lived centers is the same.

The obtained results lead to the following conclusions.

The quantum, nonthermic photon-driven adsorption, desorption and reactions are proved to exist for all studied oxides. These processes are site-sensitive and spectrally selective. The kinetic

Table 2
F-type and V-type centers as the active centers in photoadsorption/desorption

	BeO	Al_2O_3	MgO	ZnO
E_g	10.5	9.3	7.8	3.4
$\Phi_{pa\ max}$	6.6	5.5	5.1	3.1 2.4
$\Phi_{pd\ max}$	3.5	3.2		3.1
$h\nu_{max}$ abs of centers	6.6 (F), 5.4 (F^+), 3.4 (V)	5.4 (F^+), 3.1 (V^-)	5.0 (F, F^+), 2.3–1.8 (V^-)	3.1 (F^+ (V?)), 2.4 (F)

model of interaction of gas (photoadsorption) or adsorbed (photodesorption) molecules with photogenerated local centers is justified. The F-type and V-type centers are believed to be responsible for the primary act of photon absorption.

2.3. The nature of active centers

Terenin has proved the existence of active centers in Al_2O_3. Using the photoluminescence and the afterglow quenching by oxygen molecules he had demonstrated the existence of long-lived excitations [12]. However, the solid-state theory was too poor at the time for to identify the centers structures.

Centers in oxides absorbing in region $1 < h\nu < 6$ eV are numerous and different. We have observed that the shape of the spectral band of photoadsorption reproduces the shape of the light absorption by F^+ centers and practically coincides with that of the excitation band of the Al_2O_3 luminescence (Fig. 4). The quantum yield for photodesorption Φ_{pd} is of the order of 10^{-6} to 10^{-7} molecule/quantum, i.e. 10 times less than for photoadsorption Φ_{pa}, but 100–1000 times more than Φ_{pd} from metals.

The analysis of excitation and emission of photoluminescence spectra of samples photoactivated in UHV has confirmed that the photoadsorption/photodesorption active centers are indeed the photoexcited F^+ and V-centers. The dominant modes of the excitation of Al_2O_3 are:

$$F^+ + O^{2-} + h\nu \rightarrow F^* + O^- \quad (1)$$

$$V^0 + h\nu' \rightarrow V^- + h \quad (2)$$

In Eq. (1) the electron transition in F^+ results in a transfer of another electron from the valence band to form an electron donor F center and a localized hole center O^- [13], both act as the active centers in oxygen photoadsorption. Alternatively, a hole generated in the Eq. (1) causes the oxygen photodesorption.

The illumination of BeO, MgO and Al_2O_3 in the UV range under UHV at room temperature results in the afterglow (AG) persisting up to 10^3 s. The spectra of AG excitation reproduce the optical absorption bands of F^+ and F centers. However, the spectra of light emission show the luminescence not only of F^+ and F-centers (an oxygen vacancy which captured one or two electrons, respectively), but also of V^- or V-centers (metal vacancy which captured one or two holes, respectively). In the initial stage, i.e. for $t_1 - t_0$ being about some tens of seconds the kinetics of AG decay is exponential, and the emission spectra are typical of F-type centers.

Yet for $t - t_1$ in the range of 10^2 to 10^3 s the kinetics is hyperbolic $I_{ag} \propto I_1\ (t - t_1)^{-k}$, I_1 being the light intensity at t_1. For these oxides the exponent k varies from 0.95 to 1.2 that is typical of recombination process. The spectral bands of F and V-type centers (Tables 2 and 3) are distinctly revealed in AG.

Table 3
Temperature maxima and spectral features of the TSL peaks of photoexcited centers

	BeO		Al_2O_3		MgO	
T_{max} (K)	390	440	380	530	360	500
$h\nu_{em}$	3.9	3.4	4.1	2.8	4.1	2.7
Center	F		F	V	F	V

The AG is quenched when oxygen is being admitted onto the surface. As a result two types of anion radicals: O_2^- and $[O_2 \cdots O_S^-]$ appear. This "memory effect" describes the interaction of oxygen molecules with long-lived excitations. Hence, the analysis of the dependences Φ_{pa} on the gas pressure p together with the AG kinetics and the dependence of "memory effect" intensity on the spacing between the completion of illumination and gas admission allows one to calculate τ_1, τ_2. So all the three channels of excitation decay presented in Table 1 are definitively determined: the recombination of photogenerated centres z^* via radiative and non-radiative decay, as well as the adsorption of molecules on these centers.

The nature of short-lived and long-lived centers is the same, and these are the specific recombination pathways which determine the characteristic time scale of processes. It should be noted that Terenin observed long-lived luminescence of Al_2O_3 and its quenching by oxygen molecules as early as in 1936 [12].

It was discovered [14] that the value of a lot of photoreactions on ZnO and TiO_2 is more efficient in the sub-gap range than in the fundamental absorption range ($h\nu > 3.2$ eV). The low efficiency of photoadsorption under band-to-band excitation is probably due to a high efficiency of electron–hole recombination which drastically reduces the lifetime of electronic excitation in oxides. Two maxima of photoadsorption efficiency on ZnO are well pronounced at 2.4 and 3.1 eV. These maxima are typical for light absorption by F and F^+ centers in ZnO. As well, F and F^+ centers are active sites of TiO_2 irradiated in the sub-gap range [15].

So the spectro-kinetic analysis of gas phase in the [O_2/oxide + photon] system proves the existence of a non-thermal photoadsorption/desorption effect under irradiation in the sub-bandgap energy region. The primary step of photoadsorption in the sub-bandgap range – the excitation of localized F and V-type centers – is common for all investigated oxides: BeO ($E_g = 10.5$ eV), Al_2O_3 ($E_g = 9.3$ eV), MgO ($E_g = 7.8$ eV), TiO_2 ($E_g = 3.4$ eV), ZnO ($E_g = 3.2$ eV) (Table 2). Photoadsorption/desorption processes are considered as the reactions of gaseous/adsorbed molecules with active centers. For the studied oxides, the kinetic parame-

ters of active centers varied in a wide range: $10^{-5} < \tau < 10^{3}$ s, $10^{-18} < \sigma < 10^{-16}$ cm^2, $10^{-6} < \Phi_{pa} < 10^{-4}$ molecule/quantum, $10^{-7} < \Phi_{pd} < 10^{-5}$ molecule/quantum.

As we see, both photoadsorption and photodesorption effects are spectrally selective in contrast to the background of numerous absorbing centers. The F-type and V-type centers are the most active in photoadsorption/desorption and photoreactions (see below). It supports Terenin's assertion that "only photochemically active regions are thus isolated from the broad, mostly unspecific continuous absorption spectrum" (see above).

The analysis of TSL and the thermostimulated annealing of optical absorption of excited centers revealed typical temperature and spectral features of F and V-type centers [16]. Table 3 gives the temperature peaks together with the spectral maxima and a type of the center. The temperature maxima and the peak shape give the value of activation energy of the centers recombination [7].

Another mechanism takes place in the fundamental absorption region. In that case the adsorbed molecule ion O_2^- is discharged by holes, photogenerated in the bulk and then extracted onto the surface. In contrast to Al_2O_3, ZnO and TiO_2 have a sufficiently high charge density to form the Schottky barrier and band bending. That promotes the charge transfer onto the surface and a drift of electrons/holes into the sample bulk, thus weakening the electron–hole back recombination and enhancing the photodesorption/adsorption efficiency [17].

It should be noted that the parameters of photoinduced effects depend not only on the oxide type, but also on the particular specimen. An important role of contaminants and ligands of variable valency is beyond the scope of this review. However, the parameters of even "nominally pure" oxides are susceptible to previous treatments in various gases under different heating temperatures.

Thus the pretreatment of isolators BeO, MgO and Al_2O_3 in hydrogen atmosphere or in UHV under 1000 K strongly increases the intensities of photoadsorption of oxygen, of photoluminescence as well as AG and TSL. Heating in oxygen atmosphere leads to an opposite result. This way it was shown that the intensities of photoadsorption of oxygen, of photoluminescence and TSL depend on the concentration of vacancies in oxygen sublattices and of their electronic structure. It allows to govern photostimulated effects by monitoring of the surface defects at extremely low concentrations starting from 10^{-6} to 10^{-5} monolayer.

Of even greater importance is the pretreatment of semiconducting oxides ZnO and TiO_2, in which the Schottky barrier and band bending are formed due to the sufficiently high charge density. That can change not only the value of photoeffects but also their direction (photoadsorption ↔ photodesorption) as well as their spectral features. It requires sample characterization in each experiment using a lot of complementary experimental methods (see Fig. 2).

2.4. Nature of photoadsorbed species

A high sensitivity of our devices allowed to solve the principal problem of investigation of photoadsorbed oxygen species, derived from very low concentrations not exceeding $\sim 10^{-5}$ monolayer. A combined analysis of results of TD spectra, thermoprogrammed bleaching of optical absorption, ESR and isotopic exchange have revealed three oxygen species on photoactivated Al_2O_3 surface, designated as A, B, and C in Fig. 5 [18].

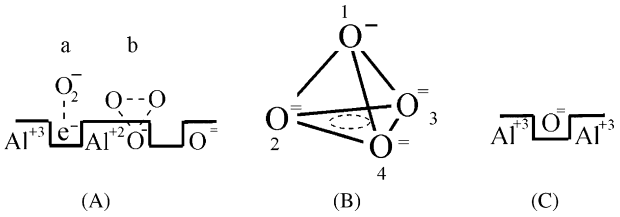

Fig. 5. Electronic and geometric structures of oxygen species on the Al_2O_3 surface.

The low-temperature peak at 380 K in TD spectra corresponds to the molecular species A. Here the molecule-surface bond is weak and E_{des} does not exceed 1 eV. The bond is provided by the charge transfer between an oxygen molecule and surface centers of F_S and/or V_S-type, thus producing O_2^- (a) and $[O_2^- \cdots O_S^-]$ (b) complexes. It results in the emergence of the absorption band of F^+ centers at 5.4 eV and of the ESR signal with $g = 2.012 \pm 0.001$. Such a signal indicates a charge transfer between the adsorbed oxygen molecule and the V_S center.

Another species B has a stronger bond between the oxygen and the surface characterized by $E_{des} = 1.2$–1.8 eV. It decays in the intermediate temperature range of $450 \leq T \leq 600$ K, just where V-type centers are decomposed (see Table 3). This species gives the UV absorption band at 3.1 eV and also the ESR signal characterized by two parameters: $g_\perp = 2.0355 \pm 0.0005$ and $g_\parallel = 2.0028 \pm 0.0005$. Such ESR signal is typical for the center with the tetrahedral symmetry. Its thermobleaching peak is close to the TSL peak at $T_{max} = 530$ K and to the thermobleaching peak of the optical absorption band at 2.9 eV [16]. So we suggest that all the three parameters characterize the same center. Its decay in the temperature range of 450–600 K causes the desorption of oxygen molecules. The photoadsorbed oxygen atom is placed in an on-top site above the surface metal vacancy which has four surface anions in the basis of the double tetrahedron. The complex is stabilized by a hole captured by one of the basis anions. The hole delocalization results in the decay of the center.

The species C (E_{des} reaching 4 eV) gives neither absorption band in the UV–vis region ($h\nu < 6$ eV), nor any ESR signal. The E_{des} value is close to that of the thermolysis energy of the surface. This species has been attributed to oxygen atoms filling anion vacancies. Thus the formation of the species C on the UV-irradiated surface allows to heal the surface defects of F-type and in this way to change the surface stoichiometry and geometry even at temperatures which are too low to activate bulk atoms.

The weak species A is responsible for the oxygen exchange with the gas phase at room temperature, the strongest species C governs the surface stoichiometry. The intermediate-bond species B maintains the equilibrium of the utmost forms A and C. Note that the species B and C are typical only for UV-irradiated samples.

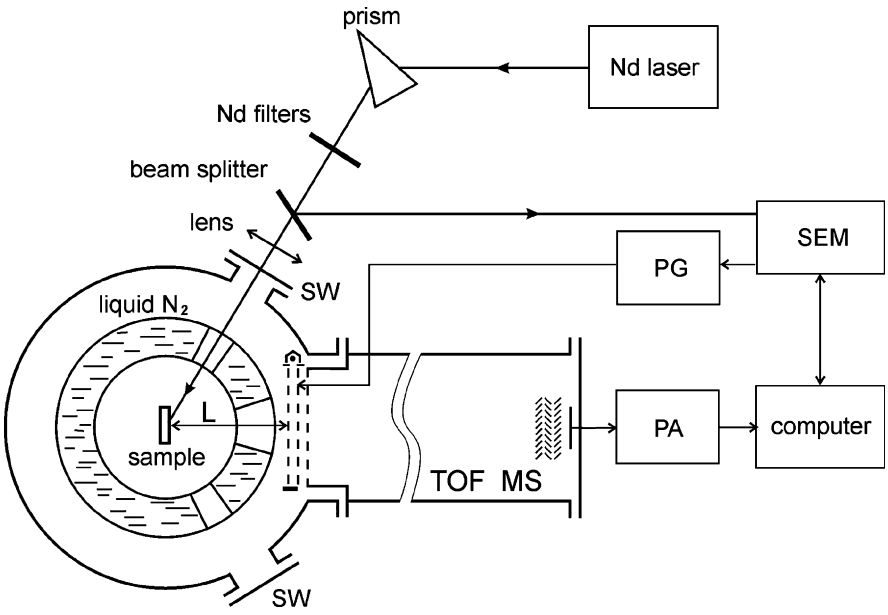

Fig. 6. Experimental setup for TOF measurements. TOF MS is the time-of-flight mass-spectrometer, PA is the preamplifier, PG is the pulse generator, SEM is the synchronized energy meter, SW is the sapphire window, *L* is the flight distance.

Similar results were obtained for the species of oxygen photoadsorbed on ZnO and TiO_2 surface and also on other wide-bandgap oxides (BeO, MgO).

A wide variety of photon-driven effects allows us to create the oxides surfaces with no influence on the bulk properties. Thus photoadsorption of oxygen allows to achieve extremely low concentrations of oxygen vacancies, i.e. below 10^{-6} monolayer. It was shown [8] that an UV–vis irradiation of a high-temperature superconducting (HTSC) single crystal of Bi2212 under UHV conditions or in oxygen atmosphere results in the photodesorption or photoadsorption of oxygen. These effects lead to the modification of the surface oxygen stoichiometry and are accompanied by a dramatic change of the electron density of states (DOS) spectra just near the E_F level [19], which is the key parameter of HTSC crystals. Similar effects were also observed on HTSC samples of YBaCuO, NdCeCuO, LaSrCuO. Also it was found that photoactivated adsorption/desorption of oxygen drastically changes the electron DOS spectra near the E_F and, as a result, the luminescence spectra of porous silicon SiO_x [20]. Modification of oxygen stoichiometry in GMR single crystals of LaSrMnO due to photoactivated adsorption/desorption of oxygen was also established. Photodesorption of oxygen species from TiO_2 surface allowed to create the heterostructure TiO_2–TiO_{2-x} on the TiO_2 surface exhibiting a very high photocatalytic activity in visible light [21].

In all cases mentioned above the key surface properties of the materials were found to be sensitive to the concentration of surface oxygen species. The oxygen could be incorporated into the surface via photoinduced adsorption, thus healing the surface defects. The opposite effect of the photoinduced desorption allows to reduce the oxidation of the surface with great care under the conditions eliminating bulk oxygen diffusion to the surface. The highly chemically active oxygen species B is of great importance in many oxidation reactions.

2.5. Dynamics of bond breaking

2.5.1. Time-of-flight spectroscopy of photodesorbed particles

Having analyzed the energetics of photodesorption Terenin has pointed out that the desorbed particle can gain the rest of the photon energy, if the latter exceeds the energy necessary for bond breaking [3]. This excess can be transformed into electronic, vibrational or kinetic mode of excitation of emitted particle. Analysis of the kinetic energy provides a deeper insight into mechanism of photodesorption.

The final step of the considered three-step process is the potential energy transformation of the electron interaction between the adsorbate and the surface into the kinetic energy of heavy nuclei. For the adsorbate photodesorption two scenarios are possible:

(1) the electron excitation energy transforms into the phonon energy of the solid, and then the excitation of the vibrational mode of the adsorbate results in the bond rupture, this process is photothermic in its nature;
(2) the electron excitation energy is transferred onto the adsorption complex, thus changing the potential energy of the adsorbate–solid interaction, which in its turn is converted into the kinetic energy of emitted particles, thus entailing the photoelectronic nature of this desorption.

These two scenarios can be discriminated in the time-resolved experiment by means of the "time-of-flight"(TOF) spectroscopy of primary products of photodesorption [22,23]. This technique is based on measuring the velocity distribution functions of particles emitted from the photoactivated surface. In the first case one can expect that the average velocity will be determined by

the surface temperature. In the second one, as it has been pointed out by Terenin, the emitted particle can gain the rest of the photon energy, which exceeds the energy necessary for bond breaking.

2.5.2. Experimental scheme and results

The experimental scheme for the time-resolved experiments is shown in Fig. 6 and has been described elsewhere [8]. The sample has been placed in a UHV chamber of the TOF mass-spectrometer at a fixed flight distance $L = 78$ mm from the ion source of the TOF mass-analyser. Up to four mass-components initiated by a single laser pulse were recorded with the time resolution equal to 10 μs. Four laser harmonics of a Q-switched Nd laser with wavelengths 1064, 532, 354 and 266 nm with the power density $P/S = 10^4$ to 10^7 W/cm^2, $\tau = 10$ ns, were used. At such power densities only single-photon excitations are possible.

The translational energy of the particles was determined from the time of flight of the distance L from the sample to the ion source:

$$\frac{dN}{dt} \sim \frac{1}{t^2}\frac{dN}{dv} = \frac{P(v)}{t^2}$$

The particles, separated according to their time of flight, were analyzed then by the TOF mass-spectrometer according to their mass values.

2.5.3. Time-of-flight spectra of oxygen desorbed from ZnO

A high sensitivity of our device allowed to study the photodesorption using a single laser pulse both in the range (*I*) of fundamental absorption of ZnO ($\lambda < 385$ nm) at $\lambda = 266$ and at 354 nm, and also in the sub-bandgap energy range (II) at $\lambda = 532$ and 1064 nm. We used non-polar surfaces of single crystal and polycrystalline ZnO powders. The oxide was baked out at 2×10^{-10} Torr and then heated for several hours at 650 K in 10^{-3} Torr of pure (99.99%) oxygen.

The desorption of neutral particles of O_2, O and Zn occurred as the cleaned ZnO surface was irradiated. The main desorbing product was molecular oxygen and its TOF spectra occurred to be different in the spectral ranges I and II. In the range of fundamental absorption "fast" molecules were desorbed and the TOF spectra could be approximated by a Maxwellian distribution with the kinetic temperature T_{Maxw} ~3200 K (Fig. 7a). In the sub-bandgap region "slow" molecules with $T_{Maxw} = 550$ K were predominant (Fig. 7b). In all cases the desorption of "fast" molecules was accompanied by the emission of "fast" oxygen and zinc atoms. The amount of atomic oxygen was 3–5% of the whole number of the molecules. The value of T_{Maxw} determined from TOF spectra reached 6000 K for oxygen and about 4500 K for zinc atoms.

A dramatic difference between T_{Maxw} values determined in above-bandgap and in sub-bandgap regions was obtained for other oxides as well (Table 4).

It has been shown that under the same excitation conditions different molecules (H_2O, CO, NO, O_2, CO_2) had their own characteristic kinetic temperatures T_{Maxw} which could considerably exceed the greatest temperature value T_S calculated for heating of the surface produced by a laser beam.

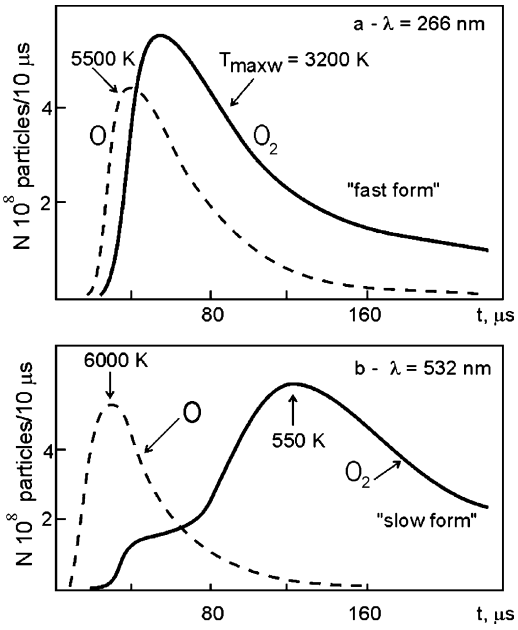

Fig. 7. Time-of-flight spectra of particles desorbed from ZnO by laser pulses of different wavelengths: (a) $\lambda = 266$ nm (bandgap energy) and (b) $\lambda = 532$ nm (sub-bandgap energy). O is the atomic oxygen; O_2 is the molecular oxygen.

We can summarize the obtained experimental results as follows [8,24]:

- the photon beams with photon energies above the bandgap energy initiate the desorption of "fast" oxygen molecules, having the kinetic temperature much higher than the surface temperature, while the desorption of "slow" molecules predominates under the excitation in the sub-bandgap ($h\nu < E_g$) range (see Table 4);
- the kinetic temperature is practically independent of the absorbed power density of the laser pulse W but is sensitive to the sample temperature;
- different desorbed molecules have their own characteristic temperatures for the same conditions of excitation;
- the number of desorbed particles rises as $N_{des} \sim (W)^n$, for "fast" molecules the exponent n being two times greater than for "slow" ones.

2.5.4. Dynamics of photon-driven desorption

Taking in mind the obtained experimental results we must rule out the photothermic model of laser desorption. Among suggested models the best agreement with the experimental results

Table 4
Photodesorption of "fast" O_2 molecules under photoexcitation in the above bandgap energy (hν > Eg) and of "slow" molecules under the excitation in the sub-bandgap (hν < Eg) range

Sample	E_g (eV)	Temperature (K) at various excitation energies (eV)			
		4.68 eV	3.51 eV	2.34 eV	1.17 eV
Cr_2O_3	1.6	2500	2500	2500	550
ZnO	3.2	3200	3200	550	550
TiO_2	3.2	3500	3500	450	400
MgO	7.9	450	450	350	350
Al_2O_3	9.2	350	350	320	320

has been obtained in the "discharge model" of O_2 photodesorption for single-photon excitations [8] (see Section 2.3). In this model the irradiation of an oxide in the sub-bandgap spectral range discharges O_2^- anions, resulting in the desorption of the "slow" molecular oxygen. Possibly there exists an intermediate precursor of a neutral complex. In this state the desorbed particle exchanges its energy with the surface and therefore "slow" molecules "follow" the temperature of the sample.

The specific features of the desorption initiated by a bandgap light absorption are caused by generation of electron–hole pairs. The simultaneous neutralization of surface oxygen and zinc ions can occur with the release of "fast" O and Zn atoms. For a desorption of "fast" oxygen molecules the recombination of two oxygen atoms is necessary. As the equilibrium distance from the surface for atomic anion O^- is shorter than for neutral oxygen, the neutralization of O^- occurs at the point lying on the repulsive branch of the potential curve for the atom–surface interaction. Thus, the potential energy of the surface–atom interaction transforms into the kinetic energy of a desorbing "fast" molecule according to the Menzel–Gomer–Redhead mechanism of desorption induced by electron transitions (DIET) [25]. The time of bond breaking ($\sim 10^{-13}$ s) is too short to remove the excess energy from the surface.

The obtained results entail the following multistep mechanisms of the photodriven desorption of oxygen from oxides:

1. Extrinsic light absorption (by a local state) followed by hole generation → excitation of the adsorbed molecular anion O_2^- → neutralization O_2^- resulting in surface–adsorbate bond breaking → desorption of "slow" O_2 molecule ("slow" form). This process can be expressed as $h + O_2^- \rightarrow O_2$ (des), where h denotes a hole.
2. Intrinsic light absorption (the fundamental one) → generation of free carrier pairs → neutralization of two oxygen anions O^- of the surface lattice. Next steps may be either a desorption of "fast" O, or a neutral atoms recombination followed by a "fast" O_2 desorption. Accordingly, in this case two single-photon excitations are required: $2h\nu + 2O^- \rightarrow O_2$(des) ("fast" form).

In the first case only adsorbed molecules of oxygen are removed from the surface, and that is why we consider such a probing as a "soft" one, useful for nondestructive diagnostics. In the second case, oxygen vacancies are created at the surface, therefore such a probing is considered as a "hard" one.

3. Photocatalysis

3.1. Photochemical reactions of oxides of nitrogen on alumina taken as a model substance for mineral dust in relation to air pollution

The oxygen photoadsorption and photodesorption are the simplest charge transfer reactions. As a more sophisticated model, the interaction of NO_x (N_2O, NO and NO_2) with γ-Al_2O_3 under the irradiation in the sub-bandgap region was studied. These experiments were aimed to simulate the reactions of these molecules with a substance of tropospheric mineral dust at low pressures typical for these pollutant molecules in the troposphere [26,27].

Two kinds of adsorption/reaction experiments were performed: (a) in quasi-static conditions under NO_x pressure at 0.001–0.1 Torr, and (b) in a flow-through regime under the equilibrium pressure in the range of 10^{-5} to 10^{-6} Torr.

Upon UV irradiation of Al_2O_3 in a N_2O flow, the composition of the gas phase markedly changed: the N_2O pressure increased due to photoinduced desorption of N_2O molecules with concomitant emergence N_2 and O_2 due to the decomposition of adsorbed N_2O. In the reaction kinetics the short-lived and long-lived centers emerge as well as in the case of photoadsorption of oxygen.

The spectral dependences of the yield of N_2O photodissociation displays a distinct maximum near ~230 nm and a shoulder at ~260 nm, just as in the case of the oxygen photoadsorption (Fig. 4). Thus, we conclude that a photoinduced decomposition of N_2O involves F^+-centers and occurs in the following reactions:

$$F^+ + h\nu \rightarrow [F^+]* \rightarrow F^{++} + e^-,$$

$$e^- + N_2O \rightarrow N_2\uparrow + O_{ads}{}^-$$

A photoinduced desorption of N_2O which proceeds in parallel with a photodissociation can be explained assuming occurrence of photostimulated decomposition of complexes that NO_x molecules can form with V-centers. The irradiation of Al_2O_3 in a NO flow by UV light in the interval of 210–300 nm leads to a NO desorption. The photoinduced desorption yield indicates the similarity of the mechanisms responsible for the photoinduced desorption of N_2O and NO.

The UV-irradiation of the NO_2–Al_2O_3 system results in an increase of NO and O_2 concentrations in the gas phase.

It is assumed that the dissociative adsorption of N_2O and NO_2, chemiluminescence and photoinduced N_2O dissociation occur via the capture of electrons from surface F- and F^+-centers of γ-Al_2O_3 by the adsorbed molecules which results in the formation of $O_{ads}{}^{2-}$ and/or $O_{ads}{}^-$ species. The photodesorption efficiency of N_2O and NO may be associated with a photoinduced decomposition of complexes formed by these molecules with surface centers.

3.2. Photocatalytic reduction of NO by CO on titanium dioxide under visible light irradiation

The titanium dioxide is widely used as a photocatalyst in the environmental catalysis at $\lambda < 385$ nm but in this case less than 3% of solar radiation is utilized. The reaction of NO on TiO_2 under UV ($\lambda < 380$ nm) irradiation was investigated in [28]. A sensitization of TiO_2 to visible light would allow to utilize about 40% of solar energy. At present, the doping of TiO_2 with noble metal ions (Pt, Ir, Rh, Au, Pd), transition metal ions (Fe, V, Cr), and non-metal ions (C, N, F, P) is used to introduce active sites able to absorb visible light [29–33].

We attempted to use intrinsic defects of non-stoichiometric TiO_{2-x} catalysts to sensitize it to visible light. As we have shown

earlier [15], the TiO_2 Degussa P-25, being reduced, absorbs light in the visible and near IR region ($400 < \lambda < 2500$ nm) due to conduction electrons and localized centers (Ti^{3+} ions, V, F and F^+ centers). An UPS study [34] revealed that the electron donor states in reduced TiO_2 fill the bandgap up to the Fermi level which lies 0.5 eV below the conduction band. So these states could take part in photon-driven processes in the visible light region. The present work aims to elucidate whether electron defects of partially reduced TiO_2 can initiate the reduction of NO by CO under visible light irradiation:

$$NO + CO \rightarrow CO_2 + \tfrac{1}{2}N_2$$

This test reaction was chosen because both gases produced in burning processes are present in polluted atmosphere.

Actually we have shown for the first time [21] that this reaction can occur on non-stoichiometric TiO_{2-x} catalysts at room temperature upon visible light irradiation ($\lambda > 380$ nm) absorbed by localized electron-donor centers (Ti^{3+} ions, V, F and F^+ centers). The selectivity of photoreduction of NO into N_2 reaches 95% and a very high stability of the catalyst activity retains. The quantum yield of NO photoreduction by CO is considerably greater for visible light irradiation ($\lambda = 405 + 436$ nm) than for UV irradiation ($\lambda = 365$ nm). However, the efficiency per one incident photon is higher in the fundamental absorption region due to a practically complete absorption of UV light.

The following stages of complete cycle are established: (a) NO photoadsorption in two parallel ways: by e^- capture from the electron-donor center by NO to yield adsorbed NO^- species, and by NO interaction with the hole O^- to give adsorbed nitrite $NO_2{}^-$; (b) reduction of NO^- into N_2O and further into N_2; and (c) photoreduction of adsorbed nitrite $NO_2{}^-$ into N_2O and its further reduction into N_2 by CO which regenerates the donor centers.

It has been found out that the photocatalytic activity of non-stoichiometric TiO_{2-x} in the visible region is associated with the presence of localized electron-donor centers (Ti^{3+} ions, V, F and F^+ centers), each electron-donor center can participate not less than 4.5 and 9 times in the formation of N_2 and CO_2, respectively.

Furthermore, it should be stressed that the reaction scheme proposed in this work allows to completely and self-consistently describe all the experimental findings observed. The scheme is also in agreement with rather abundant literature data on IR and EPR study of the NO–TiO_2 and CO–TiO_2 systems.

4. Conclusion

In conclusion we confirm that the original ideas and the fundamental results of Alexander Nikolayevich Terenin are of vital importance for any today's investigator in photophysics and photochemistry of gas–solid interface.

Acknowledgement

This work was supported by INTAS under grant 03-51-6088.

References

[1] A.N. Terenin, Uchenye zapiski LGU (rus) 3 (17) (1937) 149–168;
A.N. Terenin, Vestnik Akademii Nauk SSSR (rus) 9/10 (1938) 104–105.
[2] A.N. Terenin, Adv. Catal. 15 (1964) 227–284.
[3] A.N. Terenin, Uchenye zapiski LGU (rus) 5 (1939) 26–40;
A.N. Terenin, K.Ja. Kassparov, Acta Phys. Chim. URSS 15 (1941) 341–365.
[4] F.F. Volkenstein (Ed.), Electronnye javlenija v katalyse i adsorbtsii na poluprovodnikah (Electron Phenomena in Catalysis and Adsorption on semiconductors Lectures on Internat. Symp., Moscow, 1968), Moscow, 1969.
[5] A.N. Terenin, Yu.P. Solonitsin, Disc. Faraday Soc. 28 (1958) 28.
[6] A.N. Terenin, Photonika molecul krasitelei i rodstvennyh soedinenii (rus), Nauka, Leningrad, 1967, p. 616.
[7] X.-L. Zhou, X.-Y. Zhu, J.M. White, Surf. Sci. Rep. 13 (1991) 77.
[8] A.A. Lisachenko, Phys. Low-Dim. Struct. 7/8 (2000) 1–26;
A.A. Lisachenko, A.M. Aprelev, Tech. Phys. Lett. 21 (1995) 681.
[9] A.A. Lisachenko, F.I. Vilesov, A.N. Terenin, Doklady Akad. Nauk SSSR 160 (1965) 864–866;
M. Formenti, H. Courbon, F. Juillet, A. Lisachenko, J.R. Martin, P. Meriaudeau, S.J. Teichner, J. Vac. Sci. Technol. 9 (1971) 947;
J. Cunningham, E.L. Goold, E.M. Leahy, J. Chem. Soc., Faraday Trans. I 75 (1979) 305–313;
P. Pichat, H. Courbon, R. Enriquez, T.T.Y. Tan, R. Amal, Res. Chem. Intermed. 33 (2007) 239–250.
[10] A.A. Lisachenko, F.I. Vilesov, L.G.U. Vestnik, Phys.-Chem. 10 (1966) 30–35.
[11] A.O. Klimovskii, A.A. Lisachenko, Kinet. Katal. 32 (1991) 428;
A.O. Klimovskii, A.A. Lisachenko, Sov. J. Chem. Phys. 6 (4) (1990) 852–865.
[12] V.A. Gachkovskii, A.N. Terenin, Bull. Acad. Sci. URSS (1936) 805–832;
V.A. Gachkovskii, A.N. Terenin, Acta Physicochim. 7 (1937) 521.
[13] H. Crawford, Semicond. Insul. 5 (3) (1983) 599.
[14] L.L. Basov, G.N. Kuzmin, I.M. Prudnikov, Ju.P. Solonitsin, Uspehi Photoniki 6 (1977).
[15] A.A. Lisachenko, V.N. Kuznetsov, M.N. Zakharov, R.V. Mikhailov, Kinet. Catal. 45 (2004) 189.
[16] V.N. Kuznetsov, A.A. Lisachenko, Russ. J. Phys. Chem. 65 (1991) 1328–1334.
[17] A.A. Lisachenko, A.M. Aprelev, P.O. Artamonov, Phys. Low-Dimens. Struct. 1 (1995) 79–91;
A.A. Lisachenko, A.M. Aprelev, Tech. Phys. Lett. 21 (1995) 9.
[18] A.O. Klimovskii, T.K. Krutitskaja, A.A. Lisachenko, I.M. Prudnikov, Phys. Low-Dimens. Struct. 3/4 (1998) 167.
[19] A.M. Aprelev, V.A. Grazhulis, A.M. Ionov, A.A. Lisachenko, Physica C 235–240 (1994) 1015–1016.
[20] A.M. Aprelev, A.A. Lisachenko, R. Laiho, A. Pavlov, Y. Pavlova, Thin Solid Films 297 (1997) 142–144.
[21] A.A. Lisachenko, R.V. Mikhailov, L.L. Basov, B.N. Shelimov, M. Che, J. Phys. Chem. C 111 (2007) 14440–14447;
A.A. Lisachenko, R.V. Mikhailov, L.L. Basov, B.N. Shelimov, M. Che, High Energy Chem. (rus.), 4, Suppl., 2008 (in press);
A.A. Lisachenko, R.V. Mikhailov, L.L. Basov, B.N. Shelimov, M. Che, International Symposium on Molecular Photonics, book of abstracts, St. Petersburg, 2006, P. 55.
[22] A.A. Lisachenko, F.I. Vilesov, Zh. Tekh. Fiz. (rus) 39 (1969) 590.
[23] V.K. Ryabchuc, L.L. Basov, A.A. Lisachenko, F.I. Vilesov, Zh. Tekh. Fiz. (rus) 43 (10) (1973) 2148–2152.
[24] I.F. Moiseenko, A.A. Lisachenko, Mater. Res. Soc. Proc. 191 (1990) 1.
[25] D. Menzel, R. Gomer, J. Chem. Phys. 41 (1964) 331;
P. Redhead, Can. J. Phys. 42 (1964) 886.
[26] A.A. Lisachenko, A.O. Klimovskii, R.V. Mikhailov, B.N. Shelimov, M. Che, Appl. Catal. B: Environ. 67 (2006) 127–135.
[27] A.A. Lisachenko, A.O. Klimovskii, R.V. Mikhailov, B.N. Shelimov, M. Che, Catal. Today 119 (2007) 247–251.

[28] H. Courbon, P. Pichat, J. Chem. Soc., Faraday Trans. I 80 (1984) 3175–3185.
[29] M. Takeuchi, H. Yamashita, M. Matsuoka, M. Anpo, M. Hirao, N. Itoh, Catal. Lett. 67 (2000) 135.
[30] H. Yamashita, M. Harada, J. Misaka, M. Takeuchi, B. Neppolian, M. Anpo, Catal. Today 84 (2003) 191.
[31] S. Klosek, D. Raftery, J. Phys. Chem. B 105 (2001) 2815.
[32] S. Yin, K. Ihara, Y. Aita, M. Komatsu, T. Sato, J. Photochem. Photobiol. A 179 (2006) 105.
[33] S. Sakthivel, H. Kisch, Angew. Chem. Int. Ed. 42 (2003) 4908–4911.
[34] A.A. Lisachenko, R.V. Mikhailov, Techn. Phys. Lett. 31 (2005) 21–24.